Thermally-induced interconversions of metal-pyrimidine-4,6-dicarboxylate polymers. A structural, spectroscopic and magnetic study.

Journal:	*Inorganic Chemistry*
Manuscript ID:	ic-2008-02365w.R2
Manuscript Type:	Article
Date Submitted by the Author:	18-Feb-2009
Complete List of Authors:	Masciocchi, Norberto; Università degli Studi dell'Insubria, Dipartimento di Scienze Chimiche e Ambientali Galli, Simona; Università dell'Insubria, Dipartimento di Scienze Chimiche e Ambientali Tagliabue, Giulia; Università degli Studi dell'Insubria, Dipartimento di Scienze Chimiche e Ambientali Sironi, Angelo; Universita' di Milano, DCSSI Castillo, Oscar; University of the Basque Country, Inorganic Chemistry Luque, Antonio; University of the Basque Country, Inorganic Chemistry Beobide, Garikoitz; University of the Basque Country Wang, Wenguo; Universidad de Granada Romero, Maria; Universidad de Granada, Departamento Quimica Inorganica Barea, Elisa; Universidad de Granada, Departamento Quimica Inorganica Navarro, Jorge; Universidad de Granada, Departamento Quimica Inorganica

Thermally-induced interconversions of metal-pyrimidine-4,6-dicarboxylate polymers. A structural, spectroscopic and magnetic study.

Norberto Masciocchi,[a] Simona Galli,[a,*] Giulia Tagliabue,[a] Angelo Sironi,[b] Oscar Castillo,[c] Antonio Luque,[c] Garikoitz Beobide,[c] Wenguo Wang,[d] M.Angustias Romero,[d] Elisa Barea,[d] Jorge A.R. Navarro[d,*]

[a] Dipartimento di Scienze Chimiche e Ambientali, Università dell'Insubria, via Valleggio 11, 22100 Como (Italy)

[b] Dipartimento di Chimica Strutturale e Stereochimica Inorganica, Università di Milano, via Venezian 21, 20133 Milano (Italy)

[c] Departamento de Química Inorgánica, Facultad de Ciencia y Tecnología, Universidad del País Vasco, Apartado 644, 48080 Bilbao (Spain)

[d] Departamento de Química Inorgánica, Universidad de Granada, Av. Fuentenueva S/N, 18071 Granada (Spain)

Abstract

Continuing our work on the structural and magnetic aspects of the 1-D coordination polymers of the $[M(pmdc)(H_2O)_2]\cdot H_2O$ kind (M = Fe, Co, Ni, Cu, Zn; pmdc = pyrimidine-4,6-dicarboxylate), we have combined *ab-initio* X-ray powder diffraction methods with *in situ* thermodiffractometry and thermal analyses to characterize the selective and reversible transformation of the $[M(pmdc)(H_2O)_2]\cdot H_2O$ compounds (M = Fe, Co, Ni, Cu) into the bis-hydrated $[M(pmdc)(H_2O)_2]$ counterparts by moderate heating, which is followed by an irreversible transformation into 2-D anhydrous species. The structural features of the transient bis-hydrated species, and of the completely dehydrated one are described for M = Cu. Remarkably, the first dehydration process does not alter the 1-D nature of the $[M(pmdc)(H_2O)_2]$ chains; on the contrary, the second dehydration gives rise to the loss of the axially coordinated water molecules with a concomitant condensation of the 1-D chains into 2-D layers through ancillary carboxylate bridging groups. The magnetic properties of the anhydrous [M(pmdc)] species (M = Co, Ni, Cu) have been investigated, showing that these phases behave as 2-D Heisenberg antiferromagnets. Notably, in the case of the [Ni(pmdc)] system, a weak ferromagnetic ordering, arising from a spin canting phenomenon with a blocking temperature of 13 K, is observed.

Introduction

In recent years, several coordination polymers containing *N*-heterocycles and/or organic carboxylates have been prepared, some of them possessing interesting structural features and/or functional properties.[1] Remarkable examples within this class are species containing the pyrazole, imidazole,[2] diazine moieties and/or a variety of mono- or poly-oxo carboxylate ligands.[3] Obviously, by combining these two functions within the same organic molecules, ligands with enhanced coordination possibilities can be obtained, and new polymeric materials can be isolated, as originally demonstrated by the use of isonicotinate as a bridging ligand.[4] After this pioneering work, numerous polyfunctional ligands of this type have been proposed (see Chart I for representative examples), and widely employed, also by our group, in the construction of polymeric coordination networks lacking (loosely bound) counterions in the crystal structure cavities, thus potentially favoring functional properties such as gas sponge behavior[5] or molecular recognition.[6]

Indeed, our extensive use of (differently substituted) 2- and 4-pyrimidinolates has evidenced the easy formation of porous, hydrated materials which, upon moderate heating, afforded polycrystalline species possessing significant storage capacities toward industrial and environmentally relevant gases.[5]

To extend our work to a distinct class of polyfunctional ligands, we have exploited the commercially available 4,6-dimethyl-pyrimidine, which can be easily oxidized to the corresponding dicarboxylic acid (H_2pmdc). The latter, originally prepared by Hunt and co-workers back in 1959,[7] combines the *N*,*N'*-coordination features of pyrimidine to the donor properties of carboxylates. Moreover, possessing two easily removable acidic hydrogen atoms, it can be coupled to the M(II) ions of the transition metal series, in search for simple coordination polymers of [M(pmdc)] formulation.

Our recent results showed that the tris-hydrated species of $[M(pmdc)(H_2O)_2]\cdot H_2O$ formulation (M = Fe, Co, Zn) are typically formed by reacting the proper metal and ligand salts in aqueous/methanolic solutions.[8] As a further step of this investigation, we have prepared, and structurally characterized, the still missing polycrystalline Ni(II) and Cu(II) $[M(pmdc)(H_2O)_2]\cdot H_2O$ derivatives. It is worth noting that $[Ni(pmdc)(H_2O)_2]\cdot H_2O$ had been already isolated; yet, its modest (poly)crystallinity allowed just to postulate its isomorphism with the other tris-hydrated compounds, not a complete structural analysis.[8]

By means of *in situ* variable temperature X-ray diffraction (TXRPD), we proved that the $[M(pmdc)(H_2O)_2]\cdot H_2O$ 1-D chains ($\mathbf{1_M}$; M = Fe, Co, Ni, Cu) undergo two consecutive dehydration steps, affording the bis-hydrated, polycrystalline $[M(pmdc)(H_2O)_2]$ counterparts ($\mathbf{2_M}$) and the completely dehydrated ones ($\mathbf{3_M}$), the latter with significant structural changes leading to a 2-D

coordination network. Worthy of note, all the species were isolated as polycrystalline materials: their structural aspects have been thus disclosed by means of *ab initio* XRPD analyses. A spectroscopic and magnetic characterization of the $\mathbf{1_M}$ and $\mathbf{3_M}$ species is also presented, disclosing that the structural modifications prompted by the $\mathbf{1_M} \rightarrow \mathbf{3_M}$ transformation deeply affect the magnetic behavior.

Experimental

Synthesis

$\mathbf{1_M}$ materials were synthesized according to the method reported by us in a previous paper.[8] $\mathbf{2_M}$ and $\mathbf{3_M}$ materials were prepared by controlled heating of 200 mg of the corresponding $\mathbf{1_M}$ material in a furnace (typically) up to 403 and 503 K (heating rate 10 K min^{-1}), respectively; yield 100%. As mentioned below, much lower temperatures are required to obtain the $\mathbf{2_{Cu}}$ and $\mathbf{3_{Cu}}$ species. Elemental analyses: Calc. for $C_6H_2FeN_2O_4$, $\mathbf{3_{Fe}}$: C, 32.47, H, 0.91, N, 12.62; found C 32.72, H 0.98, N 12.92. Calc. for $C_6H_2CoN_2O_4$, $\mathbf{3_{Co}}$: C, 32.02, H, 0.90, N, 12.45; found C 32.37, H 1.00, N 12.76. Calc. for $C_6H_2NiN_2O_4$, $\mathbf{3_{Ni}}$: C, 32.06, H, 0.90, N, 12.46; found C 32.44, H 0.98, N 12.72. Calc. for $C_6H_2CuN_2O_4$, $\mathbf{3_{Cu}}$: C, 31.38, H, 0.88, N, 12.20 found. C 31.66, H 0.93, N 12.55.

Physical Measurements

Thermal analyses (TG/DTG/DTA) were performed on a TA Instruments SDT 2960 thermal analyzer in a synthetic air atmosphere (79% N_2: 21% O_2) with a heating rate of 5 °C min^{-1}. DC Magnetic measurements were performed on polycrystalline samples on a SQUID Quantum Design MPMS XL-5 in the 2-300 K temperature range applying external fields of 300 and 5000 Oe. AC magnetic susceptibility measurements were performed applying an oscillating external field of 1 Oe with a frequency of 100 Hz. Elemental analyses were carried out on a Perkin Elmer CHN Analyzer 2400 Series II. Electronic spectra on polycrystalline samples were carried out on a Varian Cary UV-vis-NIR spectrophotometer in the reflectance mode. IR spectra were recorded in the 4000-300 cm^{-1} range on a Midac FT-IR using KBr pellets.

Structural Powder Diffraction Analyses

The powdered $\mathbf{1_M}$ (M = Ni, Cu), $\mathbf{2_M}$ (M = Fe, Co, Ni, Cu) and $\mathbf{3_{Cu}}$ samples were gently ground in an agate mortar, then deposited in the hollow of an aluminum sample holder equipped with a zero-background plate. The data were collected on a Bruker AXS D8 Advance diffractometer, equipped with a linear position-sensitive Lynxeye detector, primary beam Soller

slits, and Ni-filtered Cu-Kα (λ = 1.5418 Å) radiation. The generator was operated at 40 kV and 40 mA. Long overnight runs were performed, at the proper temperature, allowing fruitful structural retrievals. Notably, among the anhydrous $\mathbf{3_M}$ species, only the copper one possessed an adequate degree of crystallinity to allow a complete structural determination. For the $\mathbf{2_{Fe}}$ and $\mathbf{3_{Cu}}$ compounds, indexing by the single value decomposition technique,[9] as implemented in the TOPAS suite,[10] allowed the determination of the crystal systems and of the lattice parameters, later confirmed by the successful structure solutions and refinements. In the case of the $\mathbf{1_M}$ species, the comparison of their diffractograms with those of the already known Fe, Co and Zn homologues allowed to highlight their isomorphism, thus providing approximate unit cells later refined by means of the Le Bail method. The same holds for the $\mathbf{2_M}$ (M = Co, Ni, Cu) species, whose unit cell was obtained starting from that of $\mathbf{2_{Fe}}$. The space groups were assigned on the basis of the systematic absences. The structure solutions were initiated by the simulated annealing technique,[11] as implemented in TOPAS, using a rigid, idealized, pmdc fragment[12] and independent metal and water oxygen atoms. When pertinent, the metal ions were fixed onto special symmetry positions and geometrical restraints were added during the final cycles of the refinement. Worthy of note, the torsion angles of the carboxylate-heterocyclic ring linkage have been ultimately refined, leading to a nearly coplanar conformation, driven by π-conjugation, in all cases but in $\mathbf{3_{Cu}}$ (see the Results and Discussion Section). The peak shapes were described by the fundamental parameters approach,[13] with the aid, when necessary, of a spherical harmonics description of the anysotropic full width at half maximum. The background was modeled by a polynomial function. An isotropic, refinable thermal parameter was assigned to the metal ions, augmented by 2.0 $Å^2$ for lighter atoms. A preferred orientation correction, in the March-Dollase formulation,[14] was introduced when necessary ($\mathbf{1_{Ni}}$, $\mathbf{1_{Cu}}$, and $\mathbf{2_{Cu}}$ [10-1]; $\mathbf{3_{Cu}}$ [011]). A summary of the crystal data and refinement parameters, together with the profile and Bragg agreement factors, is supplied in Table 1 for the $\mathbf{1_M}$ compounds and in Table 2 for the $\mathbf{2_M}$ and $\mathbf{3_{Cu}}$ ones. Crystallographic data (excluding structure factors) for the structures reported in this paper have been deposited with the Cambridge Crystallographic Data Center as supplementary publication no. CCDC 712087-712093. Copies of the data can be obtained free of charge on application to the Director, CCDC, 12 Union Road, Cambridge, CB2 1EZ, UK (Fax: +44-1223-335033; e-mail: deposit@ccdc.cam.ac.uk or http://www.ccdc.cam.ac.uk).

Thermodiffractometry

The powdered samples of the $\mathbf{1_M}$ (M = Fe, Co, Ni) and $\mathbf{2_{Cu}}$ compounds were gently ground in an agate mortar, and then deposited in the hollow of an aluminum sample holder located in a custom-made heating chamber (supplied by Officina Elettrotecnica di Tenno, Italy). The data were

typically collected, on the Bruker Axs D8 Advance diffractometer, in the 303-603 K range at 20 K per step, highlighting the structural changes due to water loss.

Results and Discussion

Synthesis and Thermal Behavior

Typically, on reacting M(II) salts (M = Fe, Co, Ni, Cu) with KHpmdc in water/methanol solutions, the tris-hydrated $[M(pmdc)(H_2O)_2]\cdot H_2O$ phases, $\mathbf{1_M}$, are isolated.

The thermal behavior of the $[M(pmdc)(H_2O)_2]\cdot H_2O$ materials (M = Fe, Co, Ni, Cu) was investigated by coupling *in situ* variable temperature X-ray diffraction (TXRPD) and thermal analyses (TG and DTA). In order to facilitate the comprehension of the following discussion, the thermal behavior of all the investigated species has been sketched in Scheme 1.

Moderate heating of the $\mathbf{1_M}$ compounds (M = Fe, Co, Ni) under nitrogen afford, progressively, two novel phases. Indeed, on raising the temperature, $\mathbf{1_{Fe}}$, $\mathbf{1_{Co}}$ and $\mathbf{1_{Ni}}$ undergo a first endothermic process interpreted, on the basis of the observed mass loss, as the evolution of one water molecule per formula unit to give the bis-hydrated $[M(pmdc)(H_2O)_2]$ species ($\mathbf{2_{Fe}}$, $\mathbf{2_{Co}}$ and $\mathbf{2_{Ni}}$, respectively). The removal of just one water molecule is substantiated by the proper weight loss in the TG trace, and possesses a structural basis: only the non coordinated water molecules, loosely interacting by means of hydrogen bonds, are removed first (see below). Worthy of note, if left in humid environments, the $\mathbf{2_{Fe}}$, $\mathbf{2_{Co}}$ and $\mathbf{2_{Ni}}$ phases restore, at a different pace, the pristine tris-hydrated $\mathbf{1_M}$ counterparts (XRPD evidence). Therefore, in order to collect meaningful diffraction data, phase constancy was guaranteed by keeping $\mathbf{2_M}$, during the whole measurement, near 403 K (see Table 2), thus preventing rehydration. Further heating of the $\mathbf{2_{Fe}}$, $\mathbf{2_{Co}}$ and $\mathbf{2_{Ni}}$ materials, promotes a second endothermic event, *i.e.* the irreversible, complete dehydration to the stable, (typically) less crystalline, [M(pmdc)] materials, with significant structural changes. Further raising of the temperature, above 623 K, induces decomposition. As a representative example, Figure 1 shows the TG and DTA traces and the corresponding thermodiffractogram of $\mathbf{1_{Fe}}$, where two separate processes, corresponding to the two quoted dehydration steps, are clearly visible. The TG/DTA traces of the other $\mathbf{1_M}$ species are available in Figure S1 of the Supplementary Material.

$\mathbf{1_{Cu}}$ constitutes in this sense an exception: indeed, either already after filtering, or at a later stage, depending on the actual environment, it tends to lose one water molecule per formula unit, affording the bis-hydrated species $\mathbf{2_{Cu}}$ (or mixtures of $\mathbf{1_{Cu}}$ and $\mathbf{2_{Cu}}$), demonstrating that also unpredictable kinetic effects are at work, possibly during nucleation. In a sufficiently humid environment, pure $\mathbf{1_{Cu}}$ may survive enough to allow a complete structural characterization. Nevertheless, the thermal investigation of the copper(II) derivatives was performed directly on the

more stable $\mathbf{2_{Cu}}$ material, directly recovered from the reaction solution: as in the case of the other $\mathbf{2_M}$ compounds, heating of $\mathbf{2_{Cu}}$ promotes the irreversible complete dehydration to $\mathbf{3_{Cu}}$.

Crystal Structures Description

$[Ni(pmdc)(H_2O)_2]\cdot H_2O$, $\mathbf{1_{Ni}}$, and $[Cu(pmdc)(H_2O)_2]\cdot H_2O$, $\mathbf{1_{Cu}}$. The isostructural species $\mathbf{1_{Ni}}$ and $\mathbf{1_{Cu}}$ crystallize in the monoclinic *C2/c* space group. Though possessing a different monoclinic space group, the previously characterized $\mathbf{1_M}$ compounds share, with $\mathbf{1_{Ni}}$ and $\mathbf{1_{Cu}}$, similar unit cell parameters (see Table S1, where the originally published cell parameters[8] have been properly transformed to allow comparison with those of the species presented in this contribution). The observed space group difference is substantiated by the fact that the [*hkl*] reflections with $h+k = 2n+1$ are clearly absent in the diffractograms of $\mathbf{1_{Ni}}$ and $\mathbf{1_{Cu}}$.

In spite of the space group difference, all the $\mathbf{1_M}$ materials share the same structural motif: as already illustrated,[8] they are composed by nearly octahedral *trans*-MN_2O_4 chromophores, two nitrogen and two oxygen atoms deriving from two bis-chelating pmdc ligands, the remaining oxygen atoms belonging to coordinated water molecules. The bridging nature of the pmdc ligands eventually yields 1-D polymeric chains, along which the metal-bound water molecules protrude normally to the polymer elongation direction. The reciprocal disposition of the chains generate cavities in which non coordinated water molecules are hosted (Scheme 2).

Insert Scheme 2 near here

Further stability is imparted to the structure by the extensive net of hydrogen bonds, mediated by uncoordinated water molecules, involving the water and carboxylate oxygen atoms of adjacent chains.

The above mentioned space group difference is somewhat unexpected, and requires a deeper comment. The coordinated water molecules are located at distances, from the metals, which depend on their ionic sizes and on the presence of other (elongating, such as Jahn-Teller) effects. The uncoordinated water molecules may either symmetrically interact with different portions of the polymeric chains (as in the *C*-centered materials), or manifest a small, *coherent*, stereochemical preference, inducing symmetry lowering (as in the $P2_1/n$ phases). The factors driving toward such a preference are not easily identifiable: apparently, it is determined by very subtle effects, likely related to the small stereochemical differences among the 1-D chains in the $\mathbf{1_M}$ crystals.

*[M(pmdc)(H$_2$O)$_2$], **2$_M$** (M = Fe, Co, Ni, Cu).* The [M(pmdc)(H$_2$O)$_2$] species are isostructural and crystallize in the monoclinic *C2/c* (M = Fe, Co, Ni) or *P2$_1$/n* (M = Cu) space groups. Again, despite this space group diversity, the structure of the Cu(II) derivative shares similar unit cell parameters (Table S1) and structural aspects as the other bis-hydrated compounds. In line with the above proposed interpretation for the **1$_M$** species, such a slight structural modification can be explained by the stereochemical features of Jahn-Teller distorted Cu(II) ions, significantly different from the nearly isotropic coordination environments of the other M(II) metal ions.

As already observed for the tris-hydrated parents, the crystal structure of all the **2$_M$** species is composed by 1-D chains of [M(pmdc)(H$_2$O)$_2$] formulation. Along the chain, each M(II) ion possesses a *trans*-MN$_2$O$_4$ pseudooctahedral stereochemistry: the equatorial positions are occupied by the nitrogen and oxygen atoms of two bis-chelating pmdc ligands, bridging metal ions 6.02-6.38 Å apart, while the apical positions are occupied by two water molecules. The chains run along [101],[15] and pack as parallel bundles, reciprocally adopting a hexagonal packing, as in the **1$_M$** compounds. Adjacent chains interact through evident hydrogen bond contacts involving the oxygen atoms of the carboxylate groups and of the water molecules (Scheme 2). Taking this hydrogen bonds network into consideration, 2-D sheets normal to [-102] are generated (Figures 2 and S2).

Insert Figure 2 near here

Finally, it is worth noting that the previously reported [Cu(pmdc)(H$_2$O)$_2$]·(H$_2$O)$_{0.2}$ derivative,[8] with 2.2 water molecules *per* asymmetric unit, is distinct from **2$_{Cu}$**. Indeed, beside possessing a slightly shorter **b** axis [12.1675(4) *vs* 12.234(3) Å], it has a different space group (*C2/c vs P2$_1$/n*, the latter being confirmed by the presence of weak *hkl* peaks, with *h+k = 2n+1*, in the diffractogram of **2$_{Cu}$**). Nevertheless, apart from the obvious changes in the site symmetries required by the distinct space groups, the structures of the [Cu(pmdc)(H$_2$O)$_2$] chains are virtually identical, and, therefore, do not require any specific comparison. Notably, the small fraction of water molecules hosted in the cavities of [Cu(pmdc)(H$_2$O)$_2$]·(H$_2$O)$_{0.2}$ may speak for a solid solution of the **1$_{Cu}$** and **2$_{Cu}$** end members, obtained upon a partial dehydration **1$_{Cu}$** allowed by adequate environmental conditions.

*[Cu(pmdc)], **3$_{Cu}$**.* [Cu(pmdc)] is the only anhydrous phase in this group of materials which showed a good-quality and easily interpretable XRPD pattern. As later discussed, its lattice metrics, of triclinic symmetry, is a definite outlier in the list of monoclinic, nearly isostructural, bis- or tri-hydrated species. Nevertheless, it is found to contain the same 1-D [Cu(pmdc)] chains. Within the

chains, the Cu(II) ions possess a square planar stereochemistry, involving two *trans*-coordinated oxygen and two *trans*-coordinated nitrogen atoms of two bis-chelating pmdc ligands, bridging metal ions about 6.0 Å apart. Coordinated water removal allows the formation of longer axial M-O interactions involving the oxygen atoms of carboxylate groups of neighboring chains, which twist their typical coplanarity with the pyrimidine ring up to 19.6(7)°. Overall, the metal centers thus possess a tetragonally elongated octahedral environment, as expected, on the basis of the Jahn-Teller effect, for a d^9 metal ion as Cu(II). The longer Cu-O_2C contacts link the [Cu(pmdc)] chains into 2-D sheets, this partially hiding the 1-D character of the pristine polymer (Figure 3 and Scheme 2). Similar (though reversible) structural rearrangements promoted by water dehydration and implying both a structure dimensionality raise and a change of the functional properties, have already been observed for homo[16] or heterobimetallic[17] coordination compounds possessing N/O-coordinating ligands.

Insert Figure 3 near here

Worthy of note, the analogous Fe(II), Co(II) and Ni(II) $\mathbf{3_M}$ materials, obtained by thermal treatment of their hydrated phases, were not of sufficient crystallinity to allow a complete structural analysis. Nevertheless, the maintenance of the octahedral environment (see below) after the loss of the coordinated water molecules is indicative of a related condensation process of the 1-D chains into 2-D layered systems. This type of condensation process has been recently reported by us in order to explain the different interconversion pathways in the [Mn(pmdc)$(H_2O)_n$] systems of variable dimensionality.[5e]

Comparative Structural Analysis

For M = Fe, Co, Ni, the partial dehydration transforming the $\mathbf{1_M}$ derivatives into the $\mathbf{2_M}$ ones implies, as expected, a symmetry increase. As a representative example of the change in metrics promoted by dehydration, comparison of the XRPD traces for $\mathbf{1_{Fe}}$ and $\mathbf{2_{Fe}}$ is reported in Figure S5. In the $\mathbf{1_M}$ materials, the axially coordinated water molecules are crystallographically independent and, as such, they are involved in distinct hydrogen bond interactions with each other, and with the carboxylate and the chlatrated water oxygen atoms. Possibly, removal of the chlatrated water molecules eliminates this asymmetry, and raises the space group symmetry to *C2/c*. In this respect, it must be pointed out that the copper derivatives behave in the opposite manner, *i.e.* the loss of water molecules determines a symmetry lowering. Although this behavior is certain, on the grounds

of powder diffraction, its interpretation is not obvious, even if it could be tentatively related to the distorted coordination sphere of Cu(II).

Thanks to the pseudo-isomorphism of the tris- and bis-hydrated species, and of the recurrence of the same [M(pmdc)] structural motif despite their degree of hydration, a comparative structural analysis can reveal some interesting features.

The behavior of the bridged M···M distances (d_{MM})[18] has been studied as a function of Shannon crystal radii for coordination VI[19] [$r_{M(II)}$, Figure 4a]. For M = Fe, Co, Ni and for the same degree of hydration, d_{MM} follows the $r_{M(II)}$ trend ($d_{NiNi} < d_{CoCo} < d_{FeFe}$). Interestingly, the bis-hydrated phases possess higher d_{MM} than the tris-hydrated ones. Since these values have been computed from XRPD data collected at temperatures ranging from 298 to 403 K, a special care was taken in comparing them. However, for linear thermal expansion coefficient of 5×10^{-5} K^{-1} (a hypothetical rather large value), only a 0.5% increase of these d_{MM} values can be estimated, well below the observed increment of up to 3%.

The copper(II) derivatives *apparently* constitute a definite outlier: indeed, the d_{MM} distances i) do not respect the general d_{MM} trend, as lower d_{MM} values than expected are observed, and ii) are practically insensitive to the hydration degree. These observations can be explained considering that the bridged M···M distances in $\mathbf{1_M}$ and $\mathbf{2_M}$ mainly depend on the equatorial M-X bond lengths; on the contrary, Shannon radii are mean values evaluated taking into consideration both equatorial and axial M-O distances. Given that the Cu(II) octahedral stereochemistry is highly tetragonally distorted, $r_{Cu(II)}$ is highly biased by the longer Cu-O axial distances and cannot be considered an adequate estimate in the evaluation of the M···M distances.

Also the behavior of the molar volume (V/Z) has been investigated as a function of the crystal radii (Figure 4b). As expected, for the same degree of hydration, V/Z nicely correlates with $r_{M(II)}$. In this case, being mean values, Shannon radii are an adequate parameter in the estimation of the volume occupied by the whole coordination sphere of the metal centre.

Insert Figure 4 near here

Electronic and Magnetic Properties

The electronic spectra of the $\mathbf{1_M}$ materials are consistent with the structural study which shows the metal ions with a N_2O_4 octahedral environment. It is also noteworthy that the thermal treatment of these systems does not alter this situation, with the $\mathbf{3_M}$ phases also possessing electronic spectra characteristic of octahedral metal centers (Table 3).

As previously shown by us, the magnetic studies performed on the 1-D $\mathbf{1_M}$ $[M(pmdc)(H_2O)_2]\cdot H_2O$ systems reveal that the pmdc bridges are very efficient to transmit an antiferromagnetic exchange between the metal centers. The structural changes that take place upon thermal treatment of the $\mathbf{1_M}$ species can also have a profound effect on the magnetic properties of the systems, depending on the relative orientation between the magnetic orbitals of the metal centres and the new established carboxylate bridge. Such a definite variation of the magnetic properties upon dehydration and consecutive structural transformation has been previously observed,[16,17] though this kind of studies is not so commonly carried out. The studies performed on the anhydrous $\mathbf{3_M}$ phases are indicative of changes in their magnetic interactions (Figures 5 and 6). As above mentioned, in the $\mathbf{3_{Cu}}$ system each copper(II) centre is connected to other two metal ions through the bisbidentate pmdc bridges occupying the equatorial positions defining in this way a 1-D polymeric chain. The two additional axial interactions with the ancillary carboxylate groups from adjacent chains that give rise to the observed 2-D crystal structure involve an axial-equatorial magnetic pathway, which has been reported to provide very weak ferromagnetic or antiferromagnetic interactions.[20] Therefore we can assume a negligible magnetic exchange through the ancillary carboxylate groups and fit its magnetic data by a numerical expression proposed for uniform copper(II) chains with antiferromagetic intrachain interactions derived through the hamiltonian $H = -J\Sigma S_i \cdot S_{i+1}$.[21] An additional term to account for the presence of paramagnetic impurities have been included. The obtained value, –38.8 cm^{-1}, matches that reported for $\mathbf{1_{Cu}}$, –38.8 cm^{-1}.

For the other metals the magnetic pathway through the ancillary carboxylate groups can not be neglected. Unfortunately, the details of the crystal structures of compounds $\mathbf{3_{Ni}}$ and $\mathbf{3_{Co}}$ are unavailable due to the poor quality of their powder X-ray diffraction patterns. Although this precludes a rigorous interpretation of their magnetic behavior, a tentative modelization of their data has been performed by means of a chain model with a main field approximation for the interchain interaction.[22] The best fit parameters, g, J and zJ' for the $\mathbf{3_M}$ series are collected in Table 3. The obtained intra- and interchain magnetic exchange parameters must be taken only as a guide about the relative strength of the magnetic coupling constants through the pyrimidine ring and the ancillary carboxylate group, respectively.

Noteworthy, in the case of $\mathbf{3_{Ni}}$, the *dc* χ_M and $\chi_M T$ values sharply increase at temperatures below 13 K (Figure 6). This sharp increment in the low temperature region and at low field strengths suggests a weak ferromagnetic ordering arising from a spin canting phenomenon. This type of behavior can be confirmed by the lowering of the observed increment for the χ_M and $\chi_M T$ values at higher external fields (5000 Oe) and by means of *ac* measurements, which show a signal in both the χ' and χ'' components centered at 13 K. The lack of hysteresis in the magnetization *vs*

applied field cycles at 2 K is indicative of a soft ferromagnet. The origin of this behavior might be attributed to a significant magnetic anisotropy of the nickel(II) ion, due to the presence, in $\mathbf{3_{Ni}}$, of tetragonally elongated coordination polyhedra,[23] as a consequence of the structural stress caused by the chains condensation.

Conclusions

We have reported here the change of the structural and physicochemical properties of a series of $[M(pmdc)(H_2O)_2]\cdot H_2O$ coordination polymers upon thermal treatment. It is noteworthy that the removal of both the crystallization and axially bound coordinated water molecules does not significantly alter the octahedral stereochemistry around the metal ions. This has been proven by XRPD on the polycrystalline $\mathbf{3_{Cu}}$ species and is also suggested by spectroscopic analyses on the other $\mathbf{3_M}$ derivatives. Nevertheless, the formation of rather compact anhydrous $[M(pmdc)]_n$ 2-D networks gives rise to a significant change in their magnetic properties. This is manifested by the occurrence of a weak ferromagnetic ordering in the $[Ni(pmdc)]_n$ phase as a probable consequence of the magnetic anisotropy induced by the presence of a distorted octahedral environment as a consequence of the structural stress caused by the chains condensation.

Supporting Information Available

Synoptic collection of the unit cell parameters of the $\mathbf{1_M}$ and $\mathbf{2_M}$ species (M = Fe, Co, Ni, Cu) (Table S1). TG and DTA traces for the $\mathbf{1_M}$ species (Figure S1). Crystal packing representation for $\mathbf{2_{Cu}}$ (Figure S2). Rietveld refinement plots for species $\mathbf{1_{Ni}}$ and $\mathbf{1_{Cu}}$ (Figure S3), $\mathbf{2_{Fe}}$, $\mathbf{2_{Co}}$, $\mathbf{2_{Ni}}$ and $\mathbf{2_{Cu}}$ (Figure S4), and $\mathbf{3_{Cu}}$ (Figure S5). Comparison of the XRPD traces for $\mathbf{1_{Fe}}$ and $\mathbf{2_{Fe}}$ (Figure S6). Comparison of the XRPD traces for $\mathbf{1_{Ni}}$–$\mathbf{3_{Ni}}$ (Figure S7).

Acknowledgements

This work was supported by the Italian MUR (PRIN2006: "Materiali Ibridi Metallo-Organici Multifunzionali con Leganti Poliazotati") and Spanish Ministerio de Ciencia e Inovación (CTQ2008-00037/PPQ). The Fondazione Provinciale Comasca is acknowledged for partial funding. G.T. thanks MUR (Progetto Giovani 2006) for a doctoral grant.

Table 1. Crystal data and refinement details for the compounds $\mathbf{1_{Ni}}$ and $\mathbf{1_{Cu}}$.

Compound $[M(pmdc)(H_2O)_2]\cdot H_2O$	$\mathbf{1_{Ni}}$ **M = Ni**	$\mathbf{1_{Cu}}$ **M = Cu**
Emp. Form.	$C_6H_8NiN_2O_7$	$C_6H_8CuN_2O_7$
fw, g mol^{-1}	278.83	283.69
Crystal system	Monoclinic	Monoclinic
SPGR, Z	*C2/c*, 4	*C2/c*, 4
a, Å	7.1662(9)	7.0188(4)
b, Å	12.036(1)	12.650(1)
c, Å	10.585(1)	10.3889(9)
α, °	90	90
β, °	96.491(7)	94.985(3)
γ, °	90	90
V, Å^3	907.1(2)	918.9 (1)
ρ_{calc}, g cm^{-3}	2.042	2.051
F(000)	568	572
μ(Cu-Kα), cm^{-1}	34.3	37.0
T, K	298(2)	298(2)
2θ range, °	10-105	10-105
Indexing Gof	25.7	26.8
N_{data}	4751	4751
N_{obs}	533	536
R_p, R_{wp}[a]	0.045, 0.070	0.078, 0.121
R_{Bragg}[a]	0.060	0.079
χ^2[a,b]	10.91	15.4
V/Z, Å^3	226.8	229.7

[a] $R_p = \Sigma_i |y_{i,o} - y_{i,c}|/\Sigma_i |y_{i,o}|$; $R_{wp} = [\Sigma_i w_i (y_{i,o} - y_{i,c})^2/\Sigma_i w_i (y_{i,o})^2]^{1/2}$; $R_{Bragg} = \Sigma_n |I_{n,o} - I_{n,c}|/\Sigma_n I_{n,o}$; $\chi^2 = \Sigma_i w_i (y_{i,o} - y_{i,c})^2/(N_{obs} - N_{par})$, where $y_{i,o}$ and $y_{i,c}$ are the observed and calculated profile intensities, respectively, while $I_{n,o}$ and $I_{n,c}$ the observed and calculated Bragg intensities. The summations run over *i* data points or *n* independent reflections. Statistical weights w_i are normally taken as $1/y_{i,o}$.

[b] These high χ^2 values *i*) are clearly the consequence of the long counting rates allowed by the use of a PSD detector, which enhances model deficiencies, and *ii*) lose their statistical meaning for a Poisson's distribution of photon counting efficiency.

Table 2: Crystal data and refinement details for the compounds $\mathbf{2_{Fe}}$, $\mathbf{2_{Co}}$, $\mathbf{2_{Ni}}$, $\mathbf{2_{Cu}}$ and $\mathbf{3_{Cu}}$.

Compound $\mathbf{[M(pmdc)(H_2O)_n]}$	$\mathbf{2_{Fe}}$ **M = Fe, n = 2**	$\mathbf{2_{Co}}$ **M = Co, n = 2**	$\mathbf{2_{Ni}}$ **M = Ni, n = 2**	$\mathbf{2_{Cu}}$ **M = Cu, n = 2**	$\mathbf{3_{Cu}}$ **M = Cu, n = 0**
Emp. Form.	$C_6H_6FeN_2O_6$	$C_6H_6CoN_2O_6$	$C_6H_6N_2NiO_6$	$C_6H_6CuN_2O_6$	$C_6H_2CuN_2O_4$
fw, g mol^{-1}	257.97	261.06	260.82	265.67	229.64
Crystal system	Monoclinic	Monoclinic	Monoclinic	Monoclinic	Triclinic
SPGR, Z	*C2/c*, 4	*C2/c*, 4	*C2/c*, 4	$P2_1/n$, 4	*P-1*, 2
a, Å	6.9726(3)	6.9701(8)	6.897(1)	7.0118(2)	5.1495(5)
b, Å	11.8600(4)	11.905(1)	11.863(1)	12.1701(4)	6.7207(6)
c, Å	10.9749(4)	10.771(2)	10.692(2)	10.3889(3)	10.380(1)
α, °	90	90	90	90	86.511(6)
β, °	92.402(2)	93.298(7)	94.111(9)	94.820(2)	100.13(1)
γ, °	90	90	90	90	108.122(7)
V, Å^3	906.76(6)	892.3(2)	872.5(3)	883.40(4)	336.07(6)
ρ_{calc}, g cm^{-3}	1.890	1.943	1.986	1.996	2.269
F(000)	520	524	528	532	452
μ(Cu-Kα), cm^{-1}	135.6	153.0	34.3	37.1	45.1
T, K	393(2)	403(2)	403(2)	298(2)	383(2)
2θ range, °	10-90	10-75	10-105	10-105	5-105
Indexing Gof	22.1	53.64	-	18.6	43.5
N_{data}	4001	3251	4751	4751	5001
N_{obs}	370	230	504	1030	776
R_p, R_{wp}[a]	0.052, 0.071	0.045, 0.060	0.015, 0.022	0.041, 0.065	0.022, 0.033
R_{Bragg}[a]	0.051	0.016	0.008	0.040	0.018
χ^2[a]	7.04	3.95	3.29	11.04	4.83
V/*Z*, Å^3	226.9	223.1	218.1	220.9	168.0

[a] $R_p = \Sigma_i |y_{i,o} - y_{i,c}|/\Sigma_i |y_{i,o}|$; $R_{wp} = [\Sigma_i w_i (y_{i,o} - y_{i,c})^2/\Sigma_i w_i (y_{i,o})^2]^{1/2}$; $R_{Bragg} = \Sigma_n |I_{n,o} - I_{n,c}|/\Sigma_n I_{n,o}$; $\chi^2 = \Sigma_i w_i (y_{i,o} - y_{i,c})^2/(N_{obs} - N_{par})$, where $y_{i,o}$ and $y_{i,c}$ are the observed and calculated profile intensities, respectively, while $I_{n,o}$ and $I_{n,c}$ the observed and calculated Bragg intensities. The summations run over *i* data points or *n* independent reflections. Statistical weights w_i are normally taken as $1/y_{i,o}$.

Table 3: Electronic and magnetic properties of compounds $\mathbf{1_M}$ and $\mathbf{3_M}$.

Compound	Δ_o, cm^{-1}	g	J, cm^{-1}	z*J*', cm^{-1}	Reference
$\mathbf{1_{Fe}}$	9700	2.15	-2.5		8
$\mathbf{1_{Co}}$	10630	-	-1.7[a]		8
$\mathbf{1_{Ni}}$	9020	2.07	-5.2		8
$\mathbf{1_{Cu}}$	15150	2.14	-32.7		8
$\mathbf{3_{Co}}$	-	2.09[a]	-1.01[a]	-1.54[a]	This work
$\mathbf{3_{Ni}}$	9020	2.17[a]	-2.34[a]	-4.73[a]	This work
$\mathbf{3_{Cu}}$	15340	2.17	-38.8		This work

[a] Theoretically obtained by ab-initio Density Functional Theory (DFT) calculations.

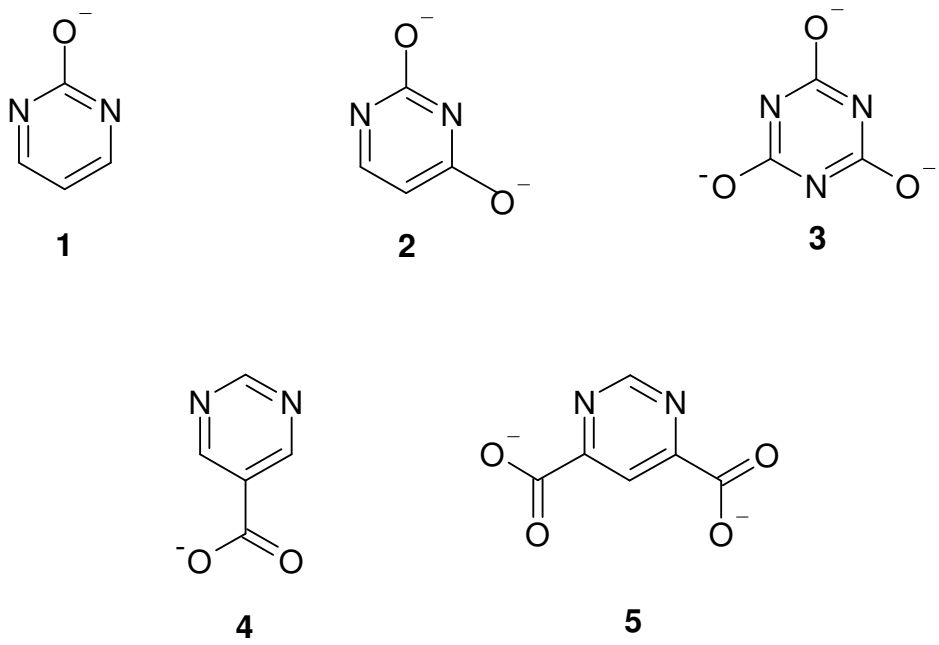

Chart I. Representative examples of anionic *N*,*O* organic ligands used in the construction of polynuclear and/or polymeric coordination complexes. 1: 2-pyrimidinolate; 2: uracilate; 3: 2,4,6-trioxo-1,3,5-triazine; 4: pyrimidine-5-carboxylate; 5: pyrimidine-4,6-dicarboxylate.

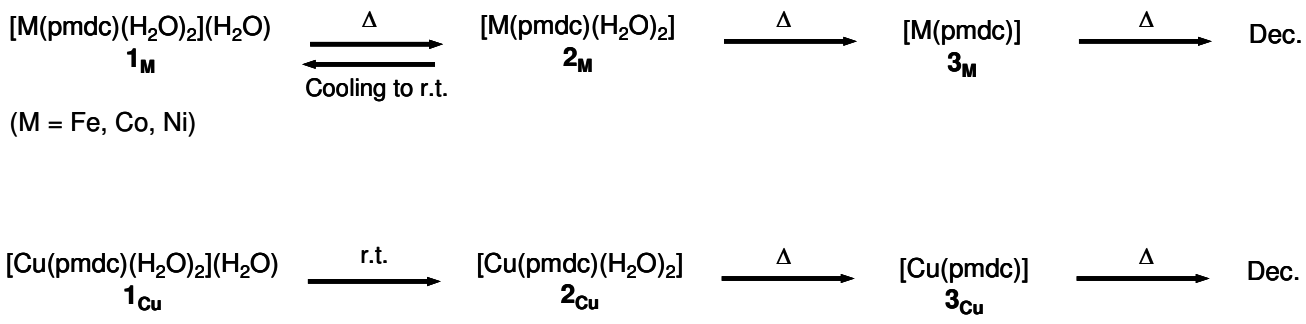

Scheme 1. Summary of the observed structural transformations for the $\mathbf{1_M}$ species, determined through a complementary use of thermodiffractometry and thermal analysis. As for the details on the relative stability of the $\mathbf{1_{Cu}}$ and $\mathbf{2_{Cu}}$ species, see text.

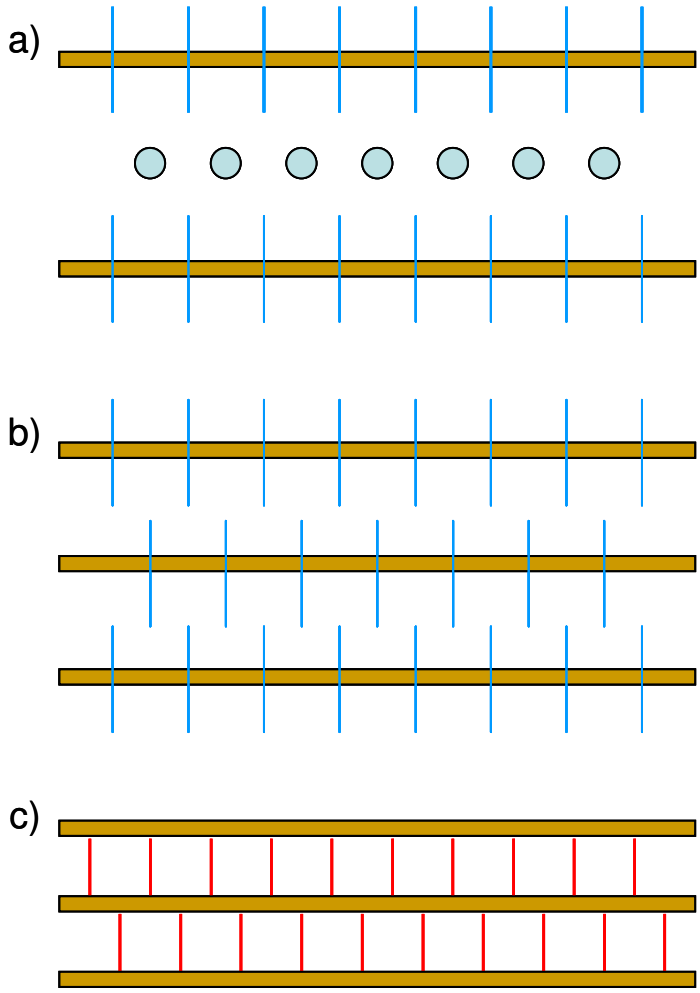

Scheme 2. Schematic representation of a) $\mathbf{1}_{Cu}$, b) $\mathbf{2}_{Cu}$ and c) $\mathbf{3}_{Cu}$ packing, showing the 1-D polymeric chains (horizontal light brown lines) and the inter-chains interactions (vertical bars) that form the overall network. Hydrogen bonds, light blue; carboxylate bridges, red; uncoordinated water molecules, turquoise circles.

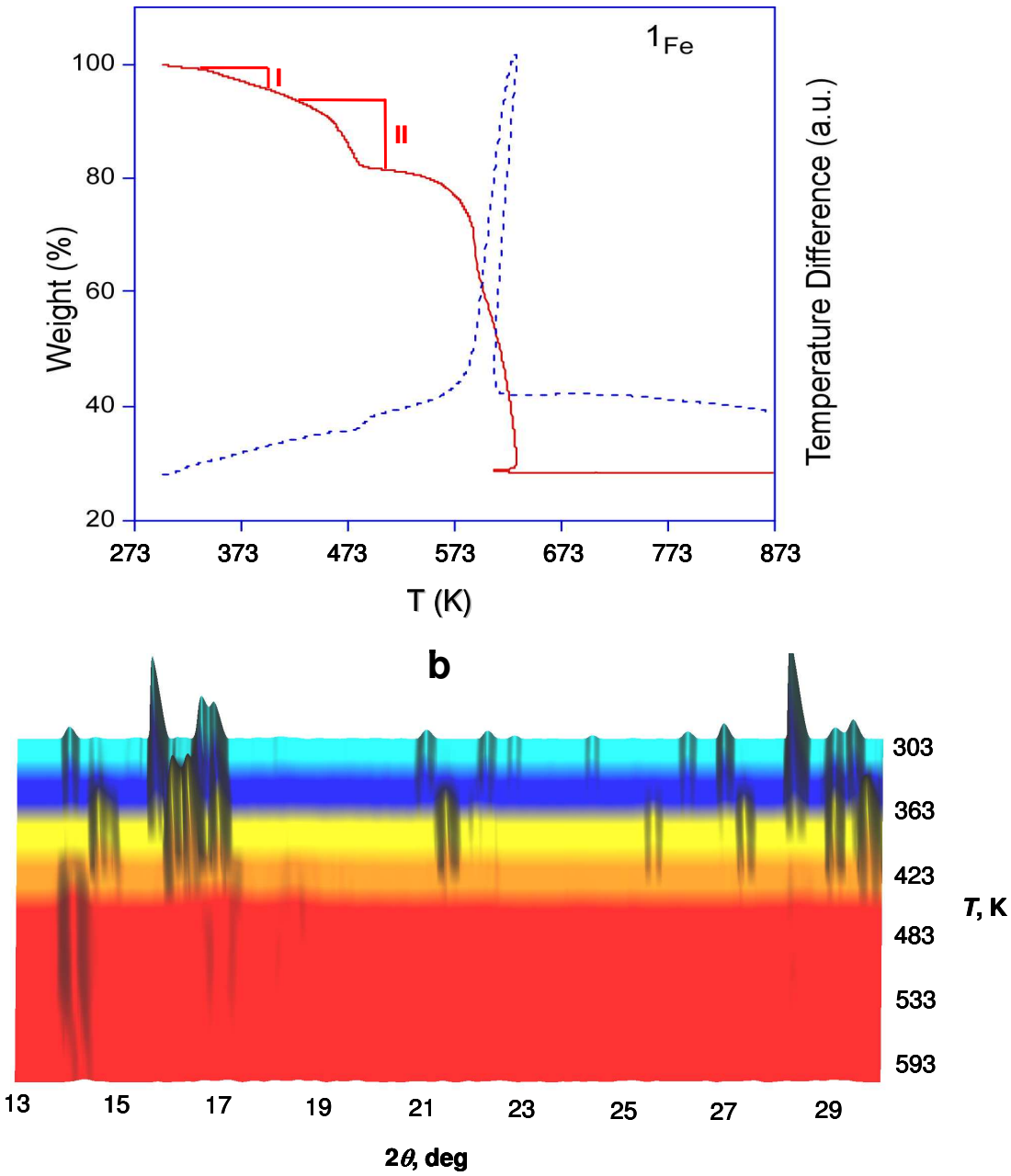

Fig. 1. Thermal behavior of $\mathbf{1}_{Fe}$. a) TG and DTA traces (red and blue, respectively); highlighted along the TG trace I) the mass loss interpreted as the evolution of the clathrated water molecule (5.9% *vs* theoretical 6.5%) and II) of the coordinated ones (10.3% *vs* theoretical 10.9%). b) Variable temperature X-ray diffractograms in the 303-623 K temperature range. The cyan, yellow and red intervals denote pure $\mathbf{1}_{Fe}$, $\mathbf{2}_{Fe}$ and $\mathbf{3}_{Fe}$, respectively, while the blue and orange ones indicate coexistence of two phases.

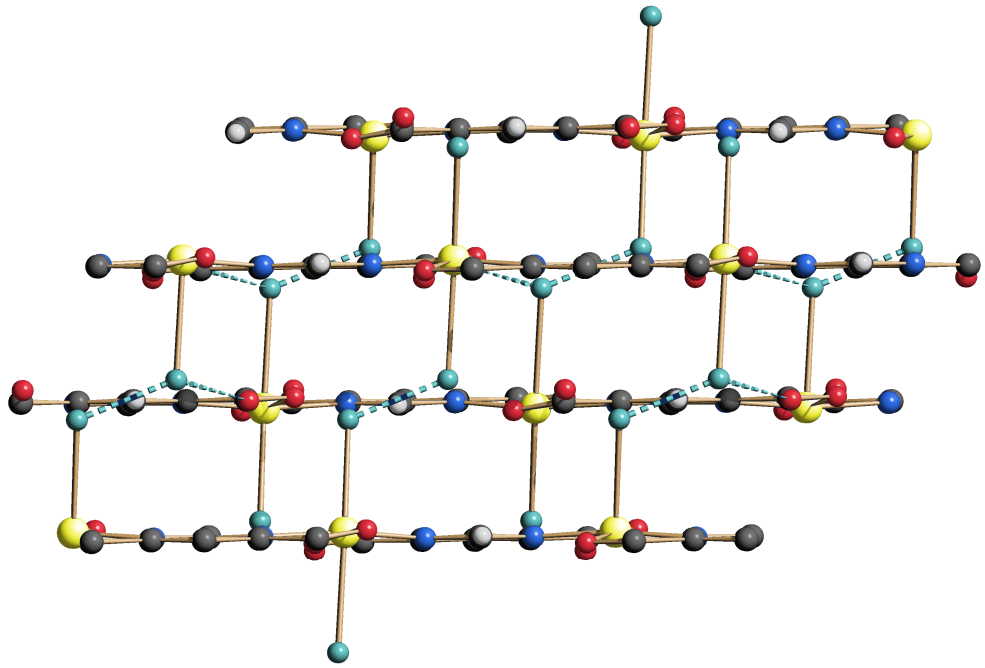

Fig. 2. Schematic drawing of the structure of compound $\mathbf{2}_{\mathbf{Cu}}$, showing the 1-D polymeric chains, and the inter-chains hydrogen bonds (dashed lines) to yield an overall 2-D network. Carbon, grey; hydrogen, light grey; nitrogen, blue; carboxylate oxygen, red; water oxygen, light blue; copper, yellow; hydrogen bonds, light blue. The structural features of the other $\mathbf{2}_{\mathbf{M}}$ species (M = Fe, Co, Ni) are, at the drawing level, undistinguishable. Significant unrestrained bond distances and angles:[24] Cu-N = 1.83(1), 2.01(1) Å; intra-chain Cu···Cu 6.02 Å; N-Cu-N = 176.5(6)°; O-Cu-O = 170.6(7)°; N-Cu-O = 89.8(4)-84.8(4)°. Hydrogen bond interactions: O1w···O2w = 2.56(1) Å; O1w···O1 = 3.01(3) Å; O2w···O1 = 2.97(2) Å; O2w···O4 = 2.85(3) Å.

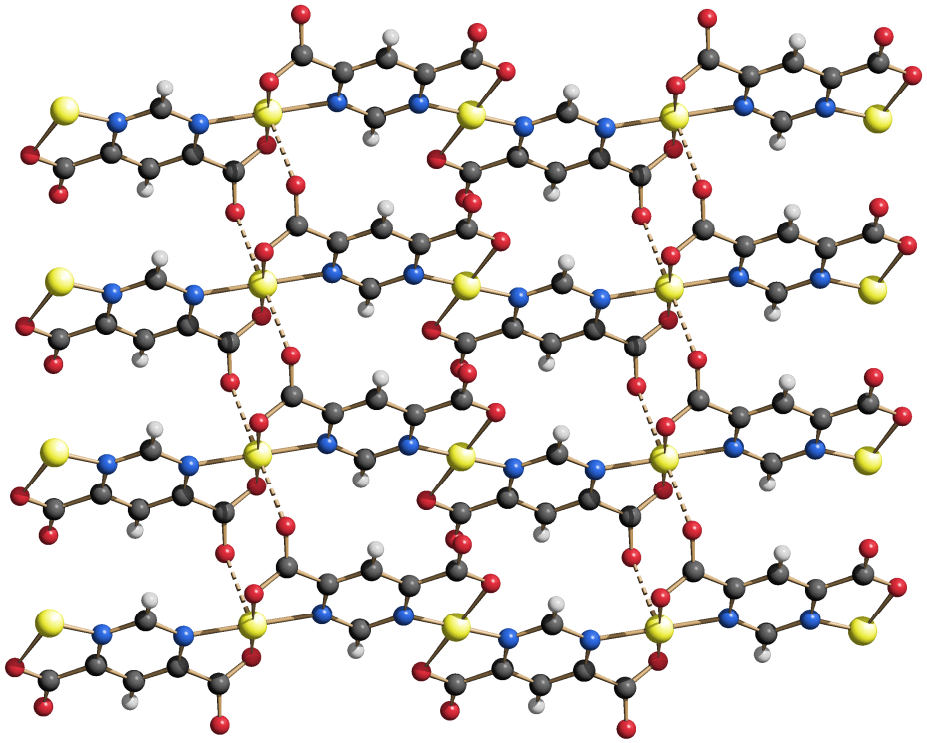

Fig. 3. Schematic drawing of structure of compound $\mathbf{3}_{\mathbf{Cu}}$, showing the 1-D polymeric chains and the longer Cu···O inter-chain contacts (dashed lines). Carbon, grey; hydrogen, light grey; nitrogen, blue; oxygen, red; copper, yellow. Significant bond distances and angles:[24] Cu-N = 1.918(7), 1.861(7) Å; Cu-O = 1.93(1), 2.02(1) Å; intra-chain Cu···Cu 6.01 Å; Cu···O = 2.86(2), 2.74(2) Å; N-Cu-O = 94.1(4)-93.7(4)°.

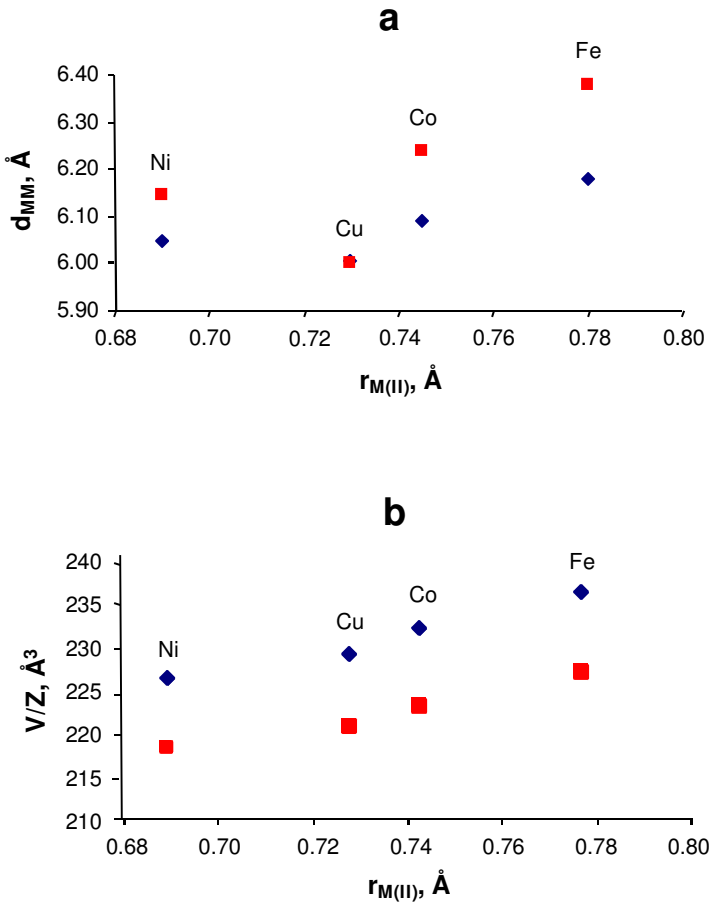

Fig. 4. Comparative structural analysis among the tris-hydrated (blue rhombi), the bis-hydrated (red squares) and the anhydrous (green circles) species: a) pmdc bridged M···M distances (d_{MM}) as a function of Shannon crystal radii for coordination number VI [$r_{M(II)}$].[19] b) Molar volume (V/Z) as a function $r_{M(II)}$.

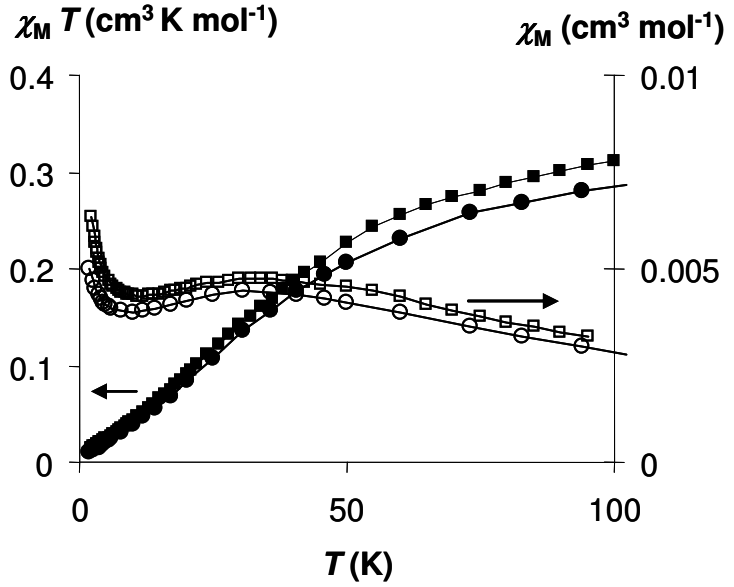

Fig. 5. Comparative thermal behaviour of the *dc* magnetic susceptibility for the $[Cu(pmdc)(H_2O)_2]\cdot H_2O$ ($\mathbf{1_{Cu}}$, circles) and [Cu(pmdc)] ($\mathbf{3_{Cu}}$, squares) phases measured applying an external magnetic field of 300 Oe. Open and full symbols denote χ_M and $\chi_M T$, respectively.

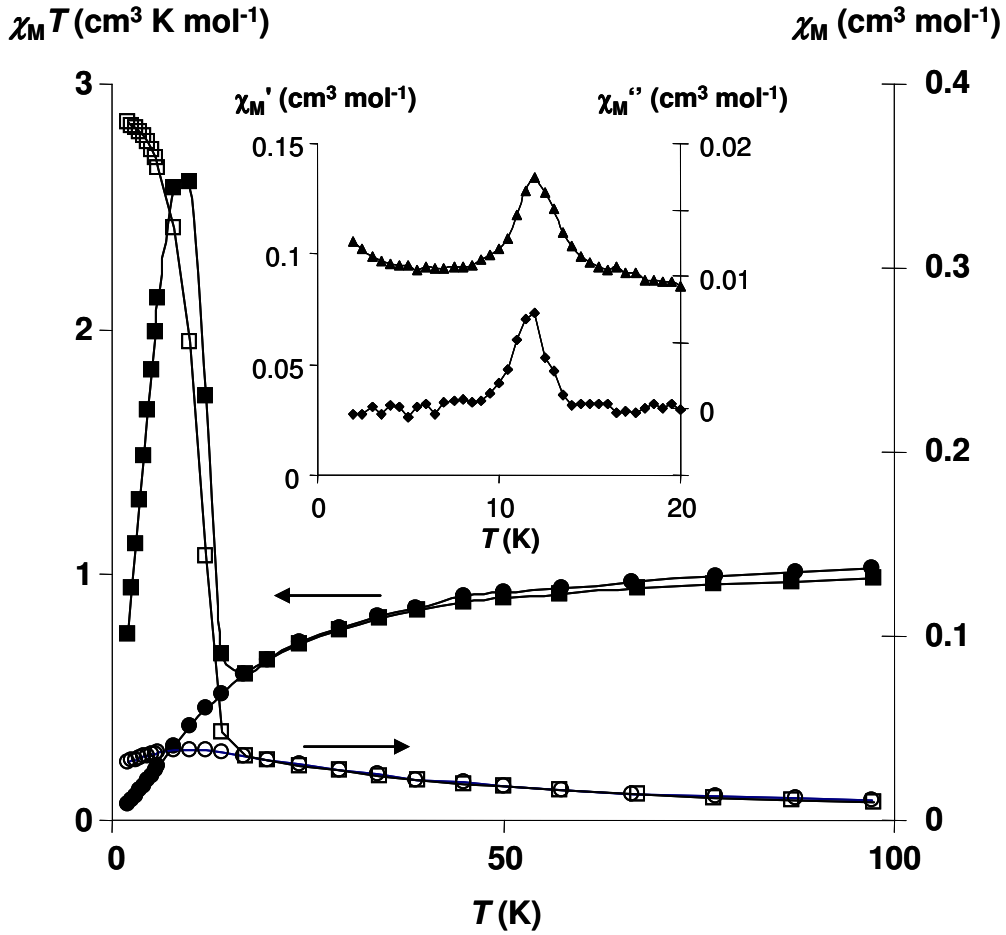

Fig. 6. Comparative thermal behavior of the *dc* magnetic susceptibility for the [Ni(pmdc)$(H_2O)_2$]·H_2O (**1**$_{Ni}$, circles) and [Ni(pmdc)] (**3**$_{Ni}$, squares) phases measured applying an external magnetic field of 300 Oe. Open and full symbols denote χ_M and $\chi_M T$, respectively. The inset in the figure represents the ac magnetic susceptibility for **3**$_{Ni}$.

Notes and References

[1] a) D. J. Collins and H.-C. Zhou, *J. Mater. Chem.*, 2007, **17**, 3154; b) S. Kitagawa, R. Kitaura and S.-I. Noro, *Angew. Chemie Int. Ed.*, 2004, **43**, 2334; c) K. Uemura, S. Kitagawa, M. Kondo, K. Fukui, R. Kitaura, H.-C. Chang and T. Mizutani, *Chem. Eur. J.*, 2002, **8**, 3587.

[2] a) K. S. Park, Z. Ni, A. P. Côté, J. Y. Choi, R. Huang, F. J. Uribe-Romo, H. K. Chae, M. O'Keeffe and O. M. Yaghi, *Proc. Natl. Acad. Sci. USA*, 2006, **103**, 10186; b) H. Hayashi, A. P. Coté, H. Furukawa, M. O'Keeffe and O. M. Yaghi, *Nat. Mater.*, 2007, **6**, 501.

[3] G. Ferey, *Chem. Soc. Rev*., 2008, **37**, 191.

[4] a) R. G. Xiong, S. R. Wilson and W. Lin, *J. Chem. Soc*., *Dalton Trans.*, 1998, 4089; b) L. Ma, O. R. Evans, B. M. Foxman and W. Lin, *Inorg. Chem.*, 1999, **38**, 5837.

[5] a) J. A. R. Navarro, E. Barea, J. M. Salas, N. Masciocchi, S. Galli, A. Sironi, C. O. Ania and J. B. Parra, *Inorg. Chem.*, 2006, **45**, 2397; b) J. A. R. Navarro, E. Barea, J. M. Salas, N. Masciocchi, S. Galli, A. Sironi, C. O. Ania and J. B. Parra, *J. Mater. Chem.*, 2007, **17**, 1939; c) A. Cingolani, S. Galli, N. Masciocchi, L. Pandolfo, C. Pettinari and A. Sironi, *Dalton Trans.*, 2006, 2479; d) J. A. R. Navarro, E. Barea, A. Rodríguez-Diéguez, J. M. Salas, C. O. Ania, J. B. Parra, N. Masciocchi, S. Galli and A. Sironi, *J. Am. Chem. Soc*., 2008, **130**, 3978; e) G. Beobide, W.-G. Wang, O. Castillo, A. Luque, P. Román, U. García-Couceiro, J. P. García-Terán, G. Tagliabue, S. Galli and J. A. R. Navarro, *Inorg. Chem.*, 2008, **47**, 5267; f) S. Galli, N. Masciocchi, G. Tagliabue, A. Sironi, J. A. R. Navarro, J. M. Salas, L. Mendez, M. Domingo, M. Perez-Mendoza and E. Barea, *Chem. Eur. J.*, 2008, **14**, 9890.

[6] a) L. C. Tabares, J. A. R. Navarro and J. M. Salas, *J. Am. Chem. Soc.*, 2001, **123**, 383; b) E. Barea, J. A. R. Navarro, J. M. Salas, N. Masciocchi, S. Galli and A. Sironi, *J. Am. Chem. Soc.*, 2004, **126**, 3014.

[7] R. R. Hunt, J. F. W. McOmie and E. R. Sayer, *J. Chem. Soc.*, 1959, 525.

[8] G. Beobide, O. Castillo, A. Luque, U. García-Couceiro, J. P. García-Terán and P. Román, *Dalton Trans.*, 2007, 2669.

[9] A. A. Coelho, *J. Appl. Cryst.*, 2003, **36**, 86.

[10] Topas-R, Bruker AXS: General profile and structure analysis software for powder diffraction data.

[11] A. A. Coelho, *J. Appl. Crystallogr.*, 2000, **33**, 899.

[12] C-C = C-N = 1.36 Å; C=O = 1.25 Å; C-H = 0.95 Å; aromatic ring angles = 120°.

[13] R. W. Cheary and A. A. Coelho, *J. Appl. Crystallogr.*, 1992, **25**, 109.

[14] a) A. March, *Z. Kristallogr.*, 1932, **81**, 285; b) W.A. Dollase, *J. Appl. Crystallogr.*, 1987, **19**, 267.

[15] The phenomenological observation of a [10-1] preferred orientation pole (introduced, for $\mathbf{2_{Cu}}$ and $\mathbf{2_{Ni}}$, in the final steps of the refinement procedure), agrees with the chain elongation axis [101], the two crystal directions being nearly normal to each other.

[16] a) X.-N. Cheng, W.-X. Zhang, Y.-Y. Lin, Y.-Z. Zeng, X.-M. Chen, *Adv. Mater.*, 2007, **19**, 1494.; X.-N. Cheng, W.-X. Zhang, X.-M. Chen, *J. Am. Chem. Soc.*, 2007, **129**, 15739.

[17] O. Kahn, J. Larionova, J. V. Yakhimi, *Chem. Eur. J.*, 1999, **5**, 3443.

[18] Worthy of note, while XRPD-derived bond distances and angles involving light atoms are inherently of low accuracy, d_{MM} interactions are typically well determined, and, therefore, can be safely employed in a relative comparison.

[19] R. D. Shannon, *Acta Cryst.*, 1976, **A23**, 751.

[20] a) O. Castillo, A. Luque, S. Iglesias, C. Guzmán-Miralles and P. Román *Inorg. Chem. Comm.*, 2001, **4**, 640; b) S. K. Ghosh, J. Ribas and P. K. Bharadwaj, *Cryst. Eng. Comm.*, 2004, **6**, 250.

[21] J. Bonner and M. E. Fisher, *Phys. Rev.*, 1964, **135**, A640.

[22] (a) C. Y. Weng, Ph.D. Thesis, Carnegie Institute of Technology, 1968. (b) A. Meyer, A. Gleizes, J. J. Girerd, M. Verdaguer, O. Kahn, *Inorg. Chem.*, 1982, **21**,1729. (c) M. E. Fisher. *Am. J. Phys.*, 1964, **32**, 343.

[23] A. Cornia, D. Gatteschi and R. Sessoli, *Coord. Chem. Rev*., 2001, **219–221**, 573.

[24] As discussed in a number of papers and reviews, bond distances and angles derived from conventional powder diffraction experiments suffer of intrinsic low accuracy, and should only be taken as semiquantitative. After all, poor data are better than no data at all.

Supplementary Material

Table S1

Synoptic collection of the unit cell parameters of the tris-hydrated $[M(pmdc)(H_2O)_2]\cdot H_2O$ and bis-hydrated $[M(pmdc)(H_2O)_2]$ species ($\mathbf{1_M}$ and $\mathbf{2_M}$ respectively in the present work; M = Fe, Co, Ni, Cu). For the sake of comparison, the unit cell parameters reported in Reference *a* have been properly transformed, this obviously implying a passage from the original $P2_1/c$ space group to $P2_1/n$.

Compound	SPGR	a (Å)	b (Å)	c (Å)	β (°)	V (Å^3)	Reference
1_M series							
$[Fe(pmdc)(H_2O)_2](H_2O)$	$P2_1/n$	7.347	12.128	10.641	95.33	944.1	*a*
$[Co(pmdc)(H_2O)_2](H_2O)$	$P2_1/n$	7.279	12.095	10.592	96.22	927.1	*a*
$[Ni(pmdc)(H_2O)_2](H_2O)$	$C2/c$	7.166	12.036	10.585	96.49	907.1	Present work
$[Cu(pmdc)(H_2O)_2](H_2O)$	$C2/c$	7.019	12.650	10.389	94.99	918.9	Present work
2_M series							
$[Fe(pmdc)(H_2O)_2]$	$C2/c$	6.973	11.860	10.975	92.40	906.8	Present work
$[Co(pmdc)(H_2O)_2]$	$C2/c$	6.970	11.905	10.771	93.30	892.3	Present work
$[Ni(pmdc)(H_2O)_2]$	$C2/c$	6.897	11.863	10.692	94.11	872.5	Present work
$[Cu(pmdc)(H_2O)_2]$	$P2_1/n$	7.012	12.170	10.389	94.82	883.4	Present work
$[Cu(pmdc)(H_2O)_2](H_2O)_{0.2}$	$C2/c$	6.977	12.234	10.391	94.93	883.7	*a*

[a] G. Beobide, O. Castillo, A. Luque, U. García-Couceiro, J. P. García-Terán and P. Román, *Dalton Trans.*, 2007, 2669.

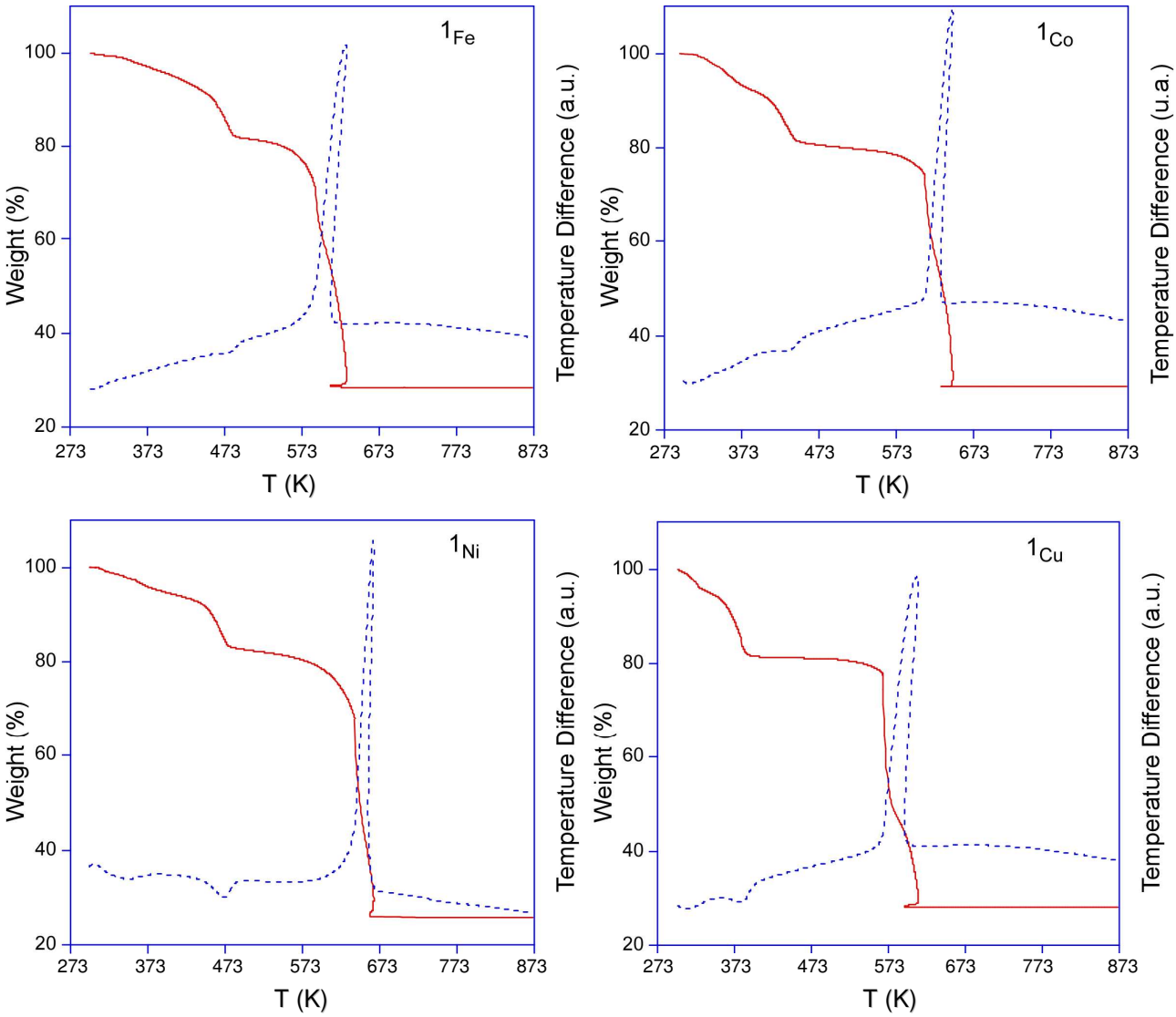

Fig. S1 Thermogravimetric curves (TG/DTA) from room temperature to 873 K.

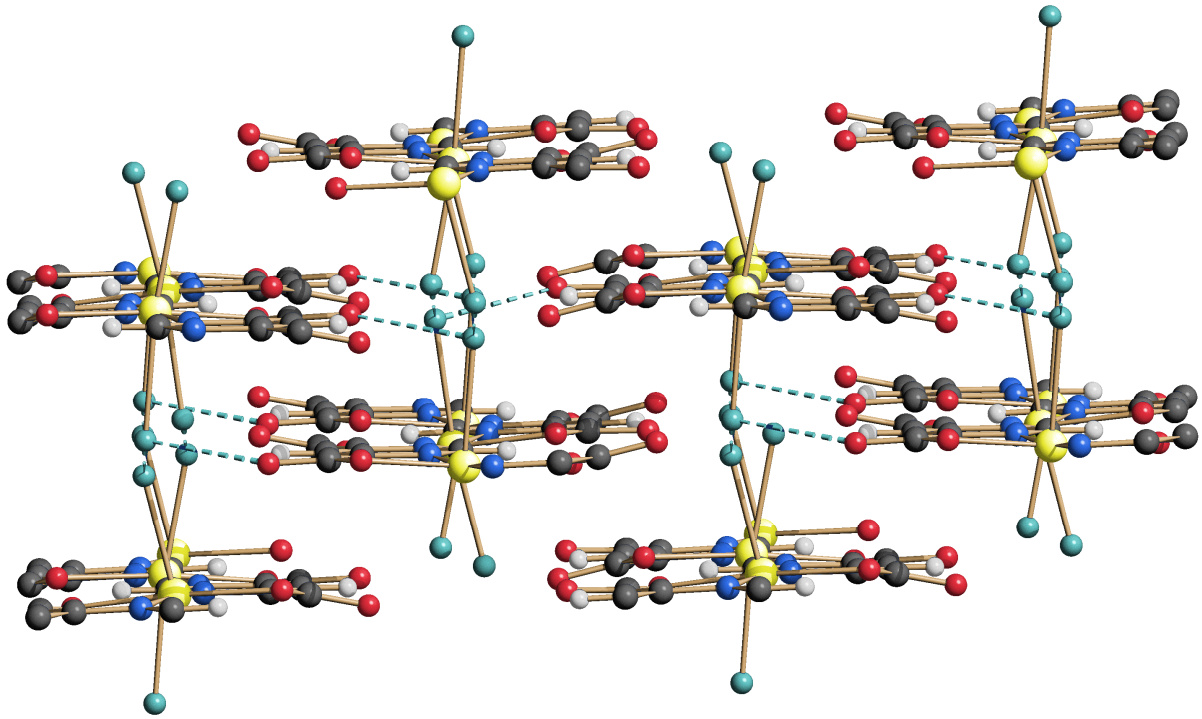

Fig. S2. Schematic drawing of the structure of compound $\mathbf{2}_{\mathbf{Cu}}$, showing the 1-D polymeric chains, orthogonal to the figure plane, and the inter-chains hydrogen bonds (dashed lines) to yield an overall 2-D network. Carbon, grey; hydrogen, light grey; nitrogen, blue; carboxylate oxygen, red; water oxygen, light blue; copper, yellow; hydrogen bonds, light blue.

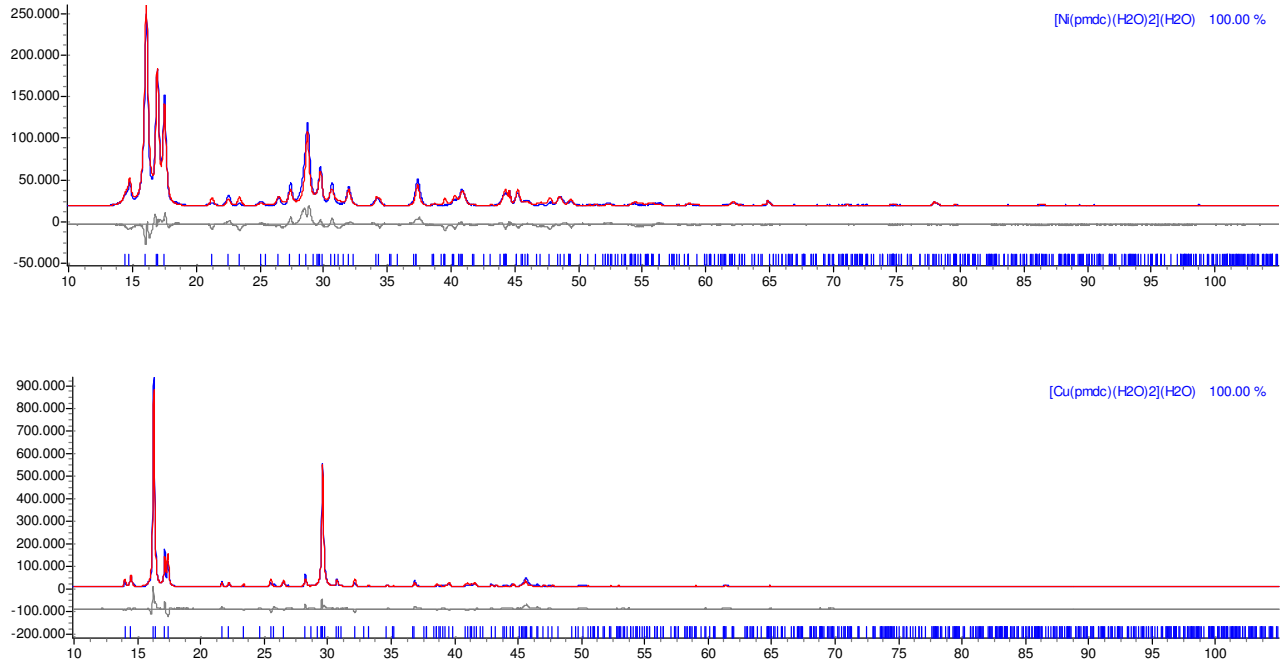

Fig. S3 Final Rietveld refinement results, in terms of experimental (blue), calculated (red), and difference (grey) plot, with peak markers at the bottom. Top to bottom: compounds $[Ni(pmdc)(H_2O)_2]\cdot H_2O$ ($\mathbf{1_{Ni}}$) and $[Cu(pmdc)(H_2O)_2]\cdot H_2O$ ($\mathbf{1_{Cu}}$). Horizontal axis: 2θ, deg. Vertical axis: intensity, counts. A few barely visible high-angle peaks in the plots of $\mathbf{1_{Ni}}$ and $\mathbf{1_{Cu}}$ are due to the aluminum sample holder.

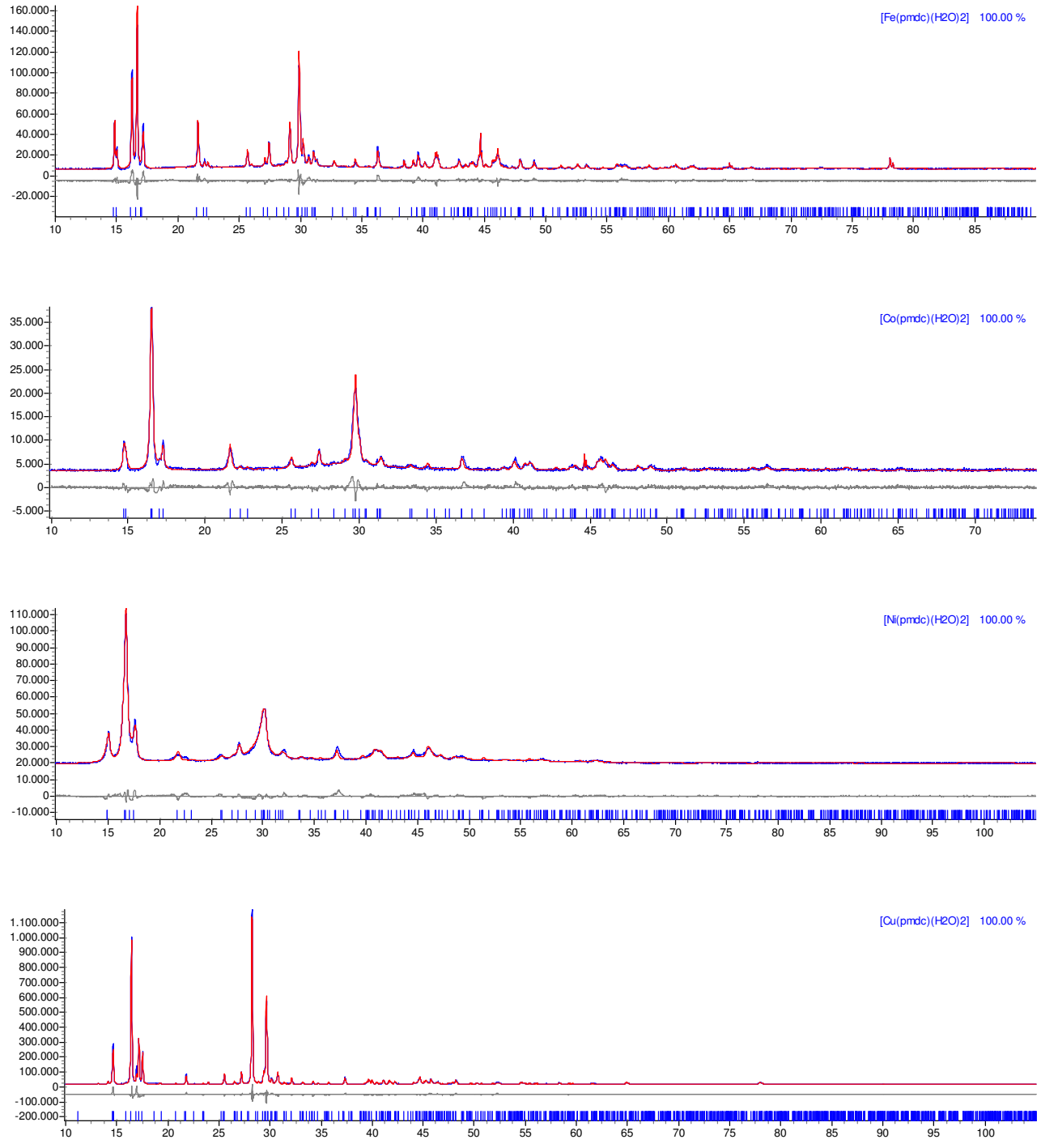

Fig. S4. Final Rietveld refinement results, in terms of experimental (blue), calculated (red), and difference (grey) plot, with peak markers at the bottom. Top to bottom: compounds $[Fe(pmdc)(H_2O)_2]$ ($\mathbf{2_{Fe}}$), $[Co(pmdc)(H_2O)_2]$ ($\mathbf{2_{Co}}$), $[Ni(pmdc)(H_2O)_2]$ ($\mathbf{2_{Ni}}$), $[Cu(pmdc)(H_2O)_2]$ ($\mathbf{2_{Cu}}$). Horizontal axis: 2θ, deg. Vertical axis: intensity, counts. A few barely visible high-angle peaks in the plots of $\mathbf{2_{Fe}}$, $\mathbf{2_{Co}}$ and $\mathbf{2_{Cu}}$ are due to the aluminum sample holder.

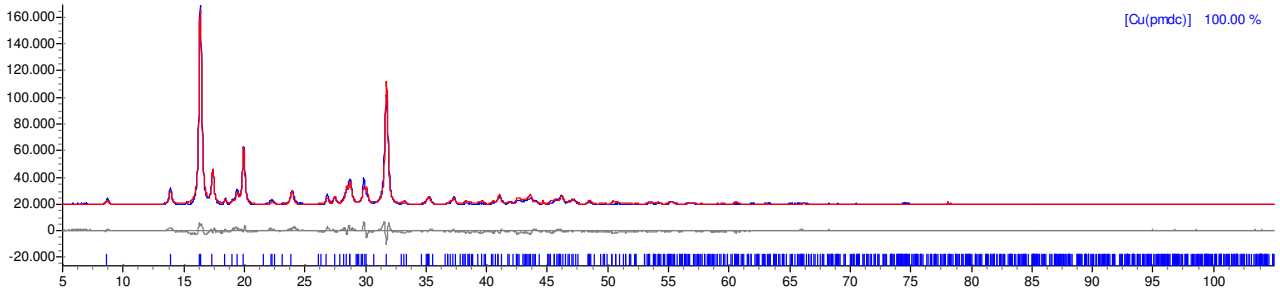

Fig. S5. Final Rietveld refinement results for [Cu(pmdc)] ($\mathbf{3_{Cu}}$), in terms of experimental (blue), calculated (red), and difference (grey) plot, with peak markers at the bottom**.** Horizontal axis: 2θ, deg. Vertical axis: intensity, counts. A few barely visible high-angle peaks in the plot are due to the aluminum sample holder.

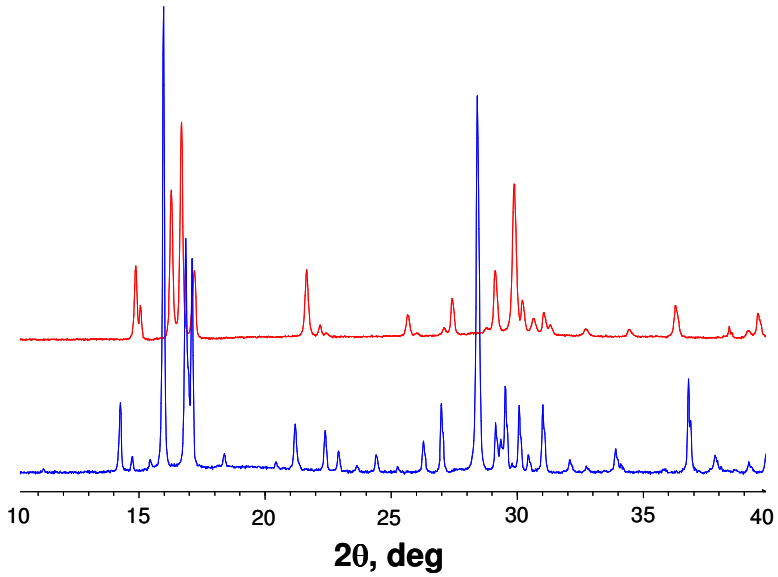

Fig. S6. Comparison of the XRPD traces of $[Fe(pmdc)(H_2O)_2]\cdot H_2O$ ($\mathbf{1_{Fe}}$, blue) and $[Fe(pmdc)(H_2O)_2]$ ($\mathbf{2_{Fe}}$, red).

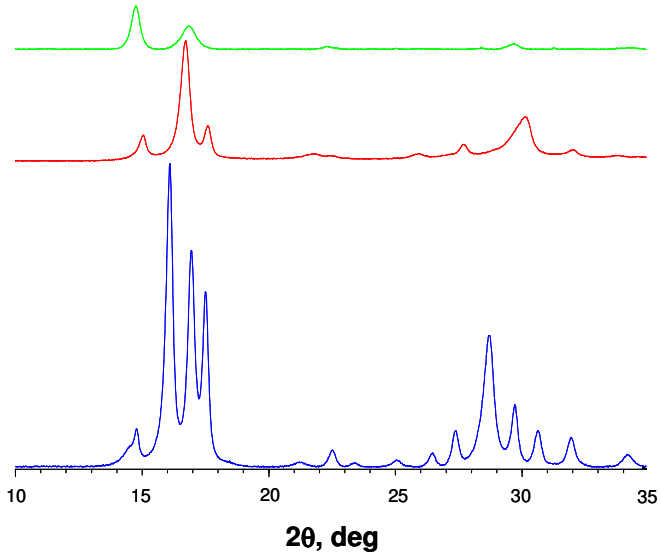

Fig. S7. Comparison of the XRPD traces of $[Ni(pmdc)(H_2O)_2]\cdot H_2O$ ($\mathbf{1_{Ni}}$, blue), $[Ni(pmdc)(H_2O)_2]$ ($\mathbf{2_{Ni}}$, red), and [Ni(pmdc)] ($\mathbf{3_{Ni}}$, green).

For the Table of Contents:

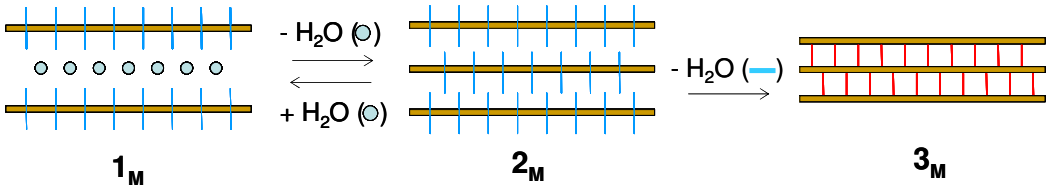

XRPD methods, combined with *in situ* thermodiffractometry and thermal analyses, highlighted the reversible transformation of the 1-D $[M(pmdc)(H_2O)_2]\cdot H_2O$ materials ($\mathbf{1_M}$, M = Fe, Co, Ni, Cu; pmdc = pyrimidine-4,6-dicarboxylate) into the 1-D bis-hydrated counterparts ($\mathbf{2_M}$) by moderate heating, followed by an irreversible complete dehydration ($\mathbf{3_M}$) implying a condensation of the 1-D chains into 2-D layers through ancillary carboxylate bridges. The magnetic characterization of $\mathbf{1_M}$ and $\mathbf{3_M}$ disclosed that the structural modifications prompted by the $\mathbf{1_M} \rightarrow \mathbf{3_M}$ transformation deeply affect the magnetic behavior.